Dalton Transactions

ROYAL SOCIETY OF CHEMISTRY

PAPER

Published on 16 July 2026
Licensed under CC-BY 4.0

Check for updates

Cite this: DOI: 10.1039/d6dt01434h

Ring extension and rearrangement reactions of an ambiphilic aluminacyclobutene

Pascal Weisenburger, [a] Israel Fernández *[b] and Frank Breher *[a]

The combination of aluminum and carbon as a Lewis acid and base, respectively, to form an intramolecular Frustrated Lewis Pair (FLP) has been less explored compared to other combinations. Herein, we present the synthesis of a metallacyclic aluminum/carbon-based ambiphile and its reactivity towards carbonyl and isocyanate compounds. The aluminacyclobutene title compound $Ph_3PCH(CH{=}CSiMe_3)AltBu_2$ (**3**) was synthesized from an alkynyl-substituted phosphonium salt $[Ph_3PCH_2C{\equiv}CSiMe_3][Br]$ (**2**) and a diorganoalanate $Li[tBu_2AlH_2]{\cdot}2thf$ (**1**). The alanate **1** is structurally characterized and applied in a hydrometallation reaction. The obtained ylide-based ambiphile **3** shows typical FLP reactivity towards carbonyl compounds resulting in ring expansion, forming $Ph_3PCH(CH{=}CSiMe_3)\{(Ph)C(H)O\}AltBu_2$ (**4**). In the reaction with phenyl isocyanate, a rearrangement reaction of the ambiphile was observed, which led to proton migration and the formation of an AlOCN heterocycle of the composition $Ph_3PC(CH{=}CHSiMe_3)\{(Ph)NCO\}AltBu_2$ (**6**). The proton shuttling initially proceeds from the ylidic carbon atom to the isocyanate's nitrogen atom providing $Ph_3PC(CH{=}CSiMe_3)\{(PhNH)CO\}AltBu_2$ (**5**), and finally to the carbon atom originally bonded to the aluminum atom. The experimental findings were rationalized through DFT calculations including an analysis of the rearrangement mechanism.

Received 11th June 2026,
Accepted 8th July 2026

DOI: 10.1039/d6dt01434h

rsc.li/dalton

Introduction

Molecular hydrides of group 13 elements are of general interest due to their use as precursors for chemical vapor deposition processes,[1] as well as for hydrometallation reactions or reductions.[2] Alanate complexes of the general composition M $[R_2AlH_2]$ (M = metal cation, R = ligand or H), like Red-Al (sodium bis(2-methoxyethoxy)aluminum hydride) or lithium aluminum hydride, are widely applicable in organic synthesis.[3] Other lithium alanate complexes bearing organic substituents are less often used due to their sensitivity and their lack of usage for hydroalumination reactions. Additionally, structural clarification has often been neglected and, therefore, only a few lithium diorganoalanates of the general composition Li $[R_2AlH_2]$, with R being a carbon-based substituent, have been structurally characterized. Up to now, only two diorganoalanates have been structurally characterized. Smith and coworkers reported the structure of the derivative $Li[tBuC(SiMe_3)_3AlH_2]{\cdot}thf$ (Chart 1) in 2003,[4] and in 2024, our group investigated the solvent-free lithium di-*tert*-butyl alanate obtained from the reaction between aluminum bromide and three equivalents of *tert*-butyl lithium (Chart 1, top).[5] To the best of our knowledge, no other diorganoalanates have been structurally analysed by SC-XRD to date. Compared to the number of alanate complexes with carbon-based substituents, nitrogen-based substituents, also in combination with carbon-based substituents, are more common.[6–10]

Group 13 element compounds are widely used as Lewis acids. One possibility to obtain ambiphilic properties of a group 13 element for potential small molecule activation would be to combine it with a Lewis base. The activation of small molecules by main group element compounds has been of general interest since the reports on metal-free dihydrogen activation by Power in 2005 and Stephan in 2006.[11,12] Combinations of Lewis bases and acids precluded from a mutual quenching, so-called Frustrated Lewis Pairs (FLPs), have since then been applied for the activation of a variety of substrates.[13–25]

Ethenylene-bridged FLPs based on aluminum and a group 15 element have been synthesized in the past by Uhl and Würthwein (**I**)[26] and later also by Mizuhata and Tokitoh (**II**) (Chart 1).[27] The aluminum/nitrogen-based FLP **I** was synthesized *via* hydroalumination starting from an alkynyl-substituted amine. This strategy was also applied later to gallanes in 2019.[28] In a similar approach, the group synthesized geminal Al/P-based FLPs before, prepared from alkynyl-substituted phosphines and diorganoalanes in 2011.[29] The ethenylene-bridged FLPs by Mizuhata and Tokitoh were obtained through

[a]*Institute of Inorganic Chemistry, Karlsruhe Institute of Technology (KIT), Engesserstr. 15, 76131 Karlsruhe, Germany. E-mail: breher@kit.edu*
[b]*Departamento de Química Orgánica and Centro de Innovación en Química Avanzada (ORFEO-CINQA), Facultad de Ciencias Químicas, Universidad Complutense de Madrid, 28040-Madrid, Spain. E-mail: israel@quim.ucm.es*

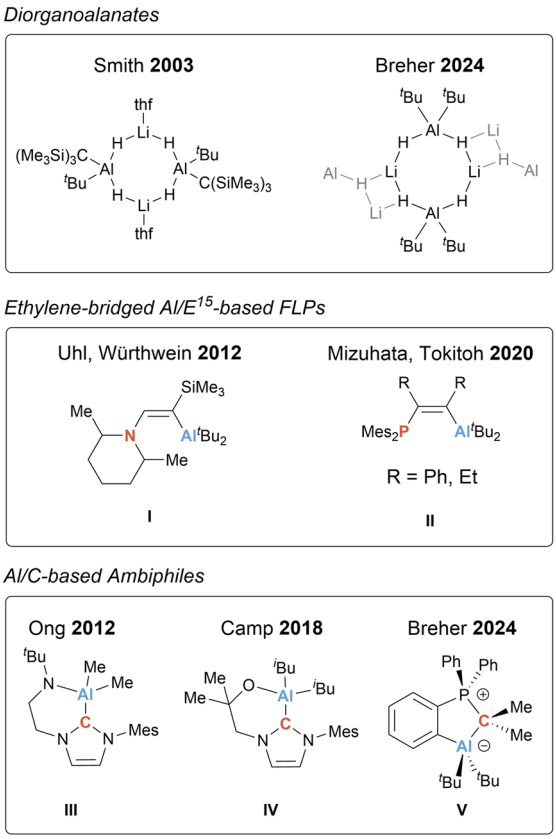

Chart 1 Top: alanate complexes by Smith and Breher;[4,5] middle: ethenylene-bridged Al/E[15]-based FLPs;[26,27] and bottom: selection of intramolecular Al/C-based ambiphiles.[31–34]

alkyne insertion into a phosphanylalane.[27] The structurally similar phenylene-bridged Al/P-based ambiphile was synthesized *via* salt metathesis and reported by our group recently.[30]

Among aluminum-based intramolecular FLPs, aluminum–carbon based systems are rare.[18] The reported systems so far include the carbene–alane adducts developed by Ong (**III**)[31] or Camp (**IV**)[32] and the *ortho*-substituted ylides such as **V** investigated by our group. The latter have been used for small molecule activation and incorporated into catalytic processes.[33–36] We found their reactivity to be limited to a few substrates and the expected FLP reactivity, for example, towards carbonyl compounds, was absent.[35] Therefore, we aimed for a different bridging unit between the ylidic carbon atom and the aluminum atom to synthesize compounds with increased reactivity.

Results and discussion

Following the strategy applied by Uhl and coworkers, we performed hydrometallation reactions with alkynyl-substituted Lewis bases. In our case, phosphorus ylides were used.[37] As ylides are generated by α-deprotonation of phosphonium salts and alanes are used for hydrometallation reactions, we used the lithium alanate Li[tBu$_2$AlH$_2$]·2thf, the formal adduct of lithium hydride and di-*tert*-butyl aluminum hydride, to perform a one-step synthesis of the aluminum-based ambiphile.

The lithium alanate Li[tBu$_2$AlH$_2$]·2thf (**1**) has been reported before by Eaborn *et al.*[38] Synthesized from LiAlH$_4$ and one equivalent of *tert*-butyl lithium, the authors described the instability of the [tBuAlH$_3$]$^-$ anion, and the solely isolable compound was Li[tBu$_2$AlH$_2$]·2thf (Scheme 1). However, the structural clarification of the alanate remained unexplored. In our attempts to determine the molecular structure *via* SC-XRD, we also obtained another structure, which is shown in the SI. The structure features six aluminium atoms in one molecule, and only four of them bear two *tert*-butyl groups; one is only bonded to one and a *tert*-butyl trihydrido alanate fragment is observed. This further indicates the rearrangement shown in Scheme 1 and can be regarded as an intermediate of the dismutation.

Targeting the diorganoalanate **1**, we used two equivalents of *tert*-butyl lithium for the reaction (Scheme 1). The reaction proceeds at room temperature overnight. The solvent is then removed, and the residue is taken up in toluene and filtered. The filtrate is again dried *in vacuo*. By recrystallization of the crude product from heptane at room temperature, we obtained single crystals of **1**. The molecular structure is shown in Fig. 1.

1 crystallizes in the monoclinic space group $C2/c$ with half a molecule in the asymmetric unit. The structure was found to be dimeric. Compared to the solvent-free analogue,[5] the bond lengths of the Al–H bonds (mean 1.62(3) Å compared to 1.55 (5) Å for **1**) are shorter, whereas the Al–C bonds are slightly elongated. The Li–H bond lengths are similar (1.83(8) Å for the solvent-free compound, 1.85(3) Å for **1**). The H–Al–H angle is expanded by 7° and the C–Al–C angle is compressed by 6°.[5] Compared to the isostructural alanate reported by Smith, the Al–H bonds are shorter (1.807(19) Å), the Al–C bond lengths are similar (2.0421(8) Å, 1.997(4) Å for **1**) and the Li–H bonds are longer (1.788 Å). The H–Al–H angle is about 3° wider for **1**, and the C–Al–C angle is about 12° compressed.[4]

We found the NMR data to slightly deviate from the reported data.[38] However, minor deviations are also observed in different batches of the synthesis. We assume that minor impurities, which we could not further identify, lead to different shifts. The singlet of the *tert*-butyl groups is observed at $\delta_{^1H}$ = 1.48 ppm. The coordinated THF molecules appear as multiplets at $\delta_{^1H}$ = 3.55 and 1.30 ppm. The hydride can be observed as a broad signal at $\delta_{^1H}$ = 2.76 ppm ($\omega_{1/2}$ = 92 Hz; Fig. 2).

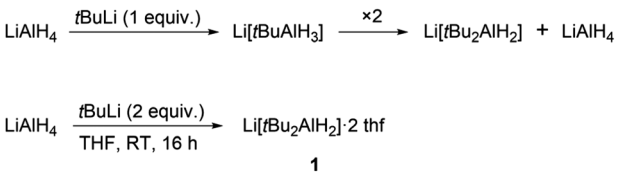

Scheme 1 Dismutation of Li[tBuAlH$_3$] according to Eaborn *et al.*[39] and synthesis of Li[tBu$_2$AlH$_2$]·2thf (**1**).

This journal is © The Royal Society of Chemistry 2026

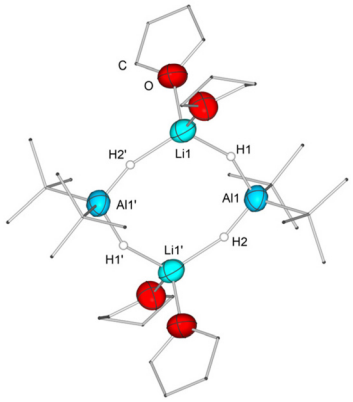

Fig. 1 Molecular structure of Li[*t*Bu$_2$AlH$_2$]·2thf (**1**; thermal ellipsoids at 30% probability). The disorder of the *tert*-butyl groups and THF molecules and all hydrogen atoms except for the hydridic ones are omitted for clarity. Selected bond lengths (Å) and angles (°): Al1–H1: 1.51(4), Al1–H2: 1.44(3), Al1–C1: 2.005(6), Al–C5: 2.001(7), Al1···Li1: 3.319(6), Li1–H1: 1.87(4), Li1–H2: 1.92(4); H1–Al1–H2: 104(2), C1–Al1–C5: 118.5(3). (We observed degradation of the single crystals of **1** upon cooling of the single crystals to temperatures lower than 250 K, most likely due to a phase transition. Therefore, the measurement was performed at 250 K and large ellipsoids were obtained for the disordered groups.)

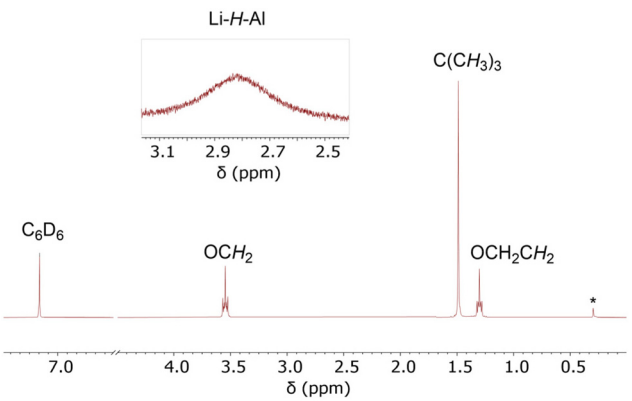

Fig. 2 ^{1}H NMR spectrum of **1** in C_6D_6. *: silicon grease.

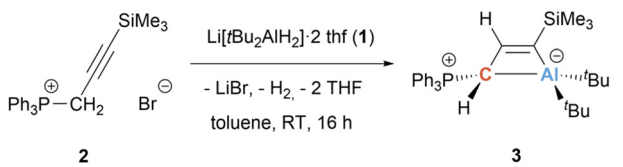

Scheme 2 Synthesis of **3** starting from **1** and **2**.

For the synthesis of the aluminum-based ambiphile (Scheme 2), **2** was synthesized *via* nucleophilic substitution of triphenylphosphine and (3-bromoprop-1-yne-1-yl)-trimethylsilane. The reaction between **1** and **2** was carried out in toluene at room temperature. After stirring for 16 hours, which led to a colour change to orange and gas evolution, evaporation of the solvent and extraction in cyclopentane, **3** was crystallized from the concentrated solution at −30 °C and obtained in moderate crystalline yields of 56%. Single crystals of **3** were obtained from the concentrated solution in cyclopentane at room temperature (space group $P2_1/c$, Fig. 3).

The Al1–C1 bond length of 2.1190(16) Å is only slightly elongated compared to compound **V** (2.118(2) Å), whereas the P1–C1 bond length is shorter (*cf.* 1.7341(15) Å for **3** and 1.800 (2) Å for **V**). Both would indicate a weaker C1–Al1 bond and a stronger P1–C1 bond. The four-membered ring is almost planar, which can be derived from the small C2–C3 torsion angle.

Density Functional Theory (DFT) calculations at the dispersion-corrected BP86-D3/def2-SVP level were carried out to gain more insight into the bonding situations of the title compound **3** and the previously reported compound **V**, featuring a four- and five-membered aluminacycle, respectively. Fig. 4 shows the corresponding QTAIM (Quantum Theory of Atoms in Molecules) Laplacian of the electron density of both species. In both cases, the systems are characterized by the occurrence of a ring critical point (RCP, red sphere), consistent with the cyclic structures. From the corresponding positive $\nabla^2\rho$ values, it is confirmed that in both cases, the Al–C bonds are donor–acceptor (*i.e.*, dative) bonds, which is consistent with the ylide nature of the carbon atoms, as reflected in their highly negative NBO charge (−1.10*e* and −0.83*e* for **3** and **V**, respectively). Interestingly, according to the delocalization indices (DI), which are considered a measure of the bond strength, the Al–C bond in **3** is slightly weaker than in **V**. Conversely, the P–C bond is slightly stronger in **V**. A similar trend is found when comparing the corresponding electron densities (ρ) at the respective bond critical points, which is consistent with the X-ray diffraction analysis (see above).

The above results suggest an increased reactivity of **3** as compared to the *ortho*-substituted ylide **V**. This is also supported by the markedly different ring strain computed using

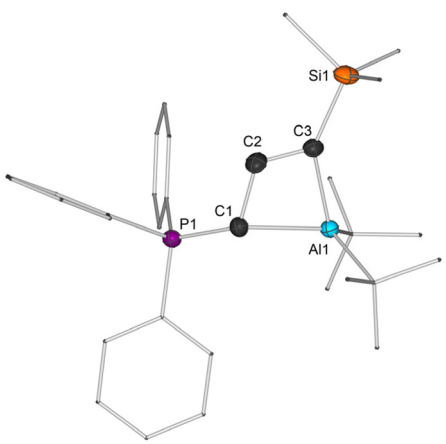

Fig. 3 Molecular structure of **3** (thermal ellipsoids at 30% probability). All hydrogen atoms and the disorder of the SiMe$_3$ group are omitted for clarity. Selected bond lengths (Å) and angles (°): Al1–C1: 2.1190(16), P1–C1: 1.7341(15), C2–C3: 1.336(2), Al1–C3: 1.9902(17), C3–Si1: 1.8380(16); C1–Al1–C3: 72.35(6), Al1–C3–Si1: 144.53(9), C1–C2–C3–Al1: 1.85(10).

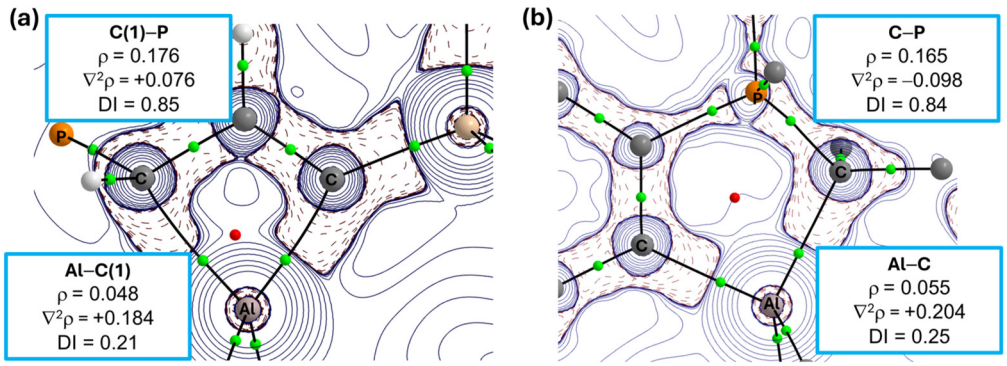

Fig. 4 Contour line diagrams $\nabla^2\rho(r)$ computed for **3** (a) and **V** (b) in the corresponding C–Al–C planes. Solid lines connecting the atomic nuclei are bond paths, while the small green and red spheres indicate the corresponding bond critical points and ring critical points, respectively.

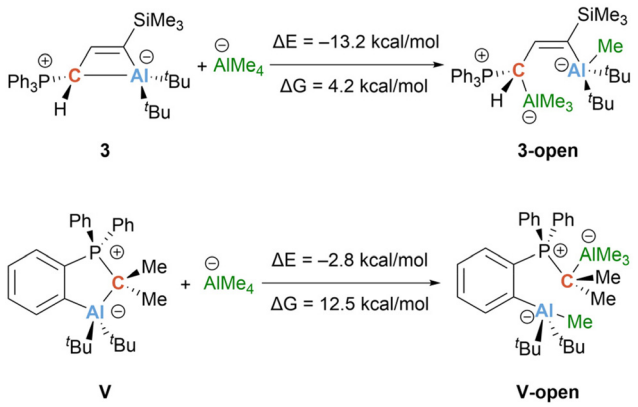

Scheme 3 Isodesmic reactions involving the ring-opening in compounds **3** and **V**.

the isodesmic reactions depicted in Scheme 3. Thus, it is found that the ring-opening reaction involving **V** is significantly more endergonic (ΔG = 12.5 kcal mol^{-1}) than the analogous process involving **3** (ΔG = 4.2 kcal mol^{-1}), which indicates an enhanced reactivity of the latter, more strained species. Nonetheless, it is known that even stable Lewis adducts, without significant "open" character, can show FLP-type reactivity, which has been shown by Fontaine and coworkers.[40,41]

3 does not show any reactivity towards dihydrogen. Treatment of **3** with carbon dioxide led to a mixture of products, which could not further be analyzed.

When a solution of **3** in deuterated benzene was treated with a stoichiometric amount of benzaldehyde (Scheme 4), the reaction mixture turned yellow. After some hours, a white precipitate was formed.

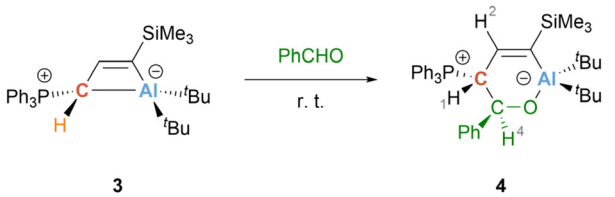

Scheme 4 Reactivity of **3** towards PhCHO.

The ^{1}H NMR spectrum indicated the insertion of the carbonyl function into the ring, forming a six-membered ring. Three concise signals – a doublet of doublets of doublets at $\delta_{^1H}$ = 4.43 ppm (H1), a doublet at $\delta_{^1H}$ = 5.51 (H2) ppm and a doublet of doublets at $\delta_{^1H}$ = 7.16 ppm (H4) – resulting from the coupling between H1, H2, H4 and P1 confirmed the insertion product (see Fig. 5). Additionally, the *tert*-butyl groups split into two singlets. Single crystals of **4** were obtained from a concentrated solution of **4** in acetonitrile (space group $P2_1$, Flack parameter = 0.08(8), Fig. 6).

Compared to **3**, the P1–C1 bond length is elongated to the typical bond length of a P–C single bond and the C4–O1 bond length equals approximately the sum of the single bond covalent radii of C and O.[42] The formed six-membered ring shows a half-chair conformation.

Next, we were interested in the ambiphile's reactivity towards isocyanates. Owing to the two polar double bonds of isocyanates, different regioisomers can be obtained from the reaction with ambiphiles. Some examples from the literature are compiled in Scheme 5. The Al/N-ambiphile **I** reacts with

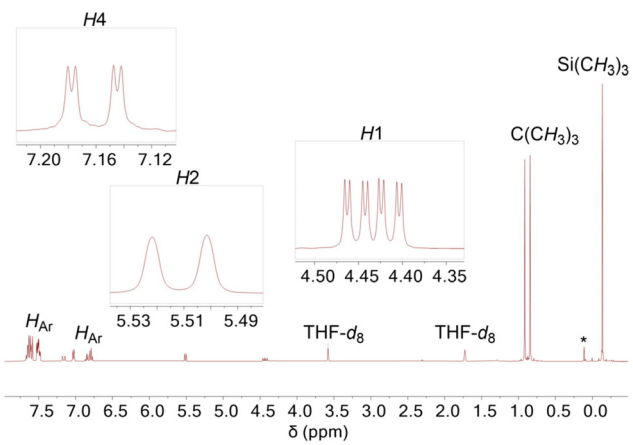

Fig. 5 ^{1}H NMR spectrum of **4** in THF-d_8. *: silicon grease. Numbering of the H atoms is according to Scheme 4.

This journal is © The Royal Society of Chemistry 2026

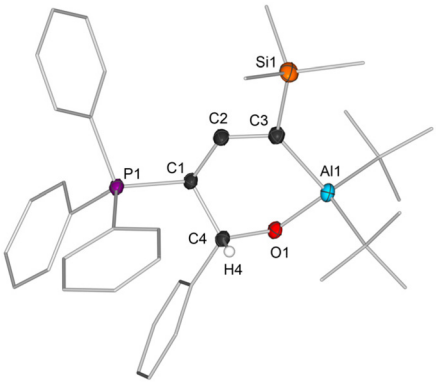

Fig. 6 Molecular structure of **4** in the solid state (thermal ellipsoids at 30% probability). The disorder of the phenyl groups is bonded to P1 and the hydrogen atoms are not shown for clarity. Selected bond lengths (Å) and angles (°): P1–C1: 1.8447(17), C2–C3: 1.347(3), Al1–C3: 2.028(2), C3–Si1: 1.873(3), C1–C4: 1.560(3), C4–O1: 1.400(4); C3–Al1–O1: 98.57 (9), Al1–C3–Si1: 134.32(11), C1–C4–O1: 108.37(18), Al1–C3–C2–C1: 5.9 (4), C1–C4–O1–Al1: 72.30(19).

phenyl isocyanate under elimination of ethynyl-trimethylsilane. When two equivalents of the isocyanate were used, insertion of a C–O function into the four-membered ring was observed.[43] Overall, the coordination of the Lewis base to the electrophilic carbon center and the concurrent coordination of the nitrogen and the oxygen atom to the Lewis acid are observed. Similar structures were obtained for the α-borylated ylides, reported by our group.[44] The gallium analogue to **I**, on the other hand, reacted with phenyl isocyanate under insertion into one carbon–gallium bond. A second equivalent can again be inserted into the four-membered ring.[28] For the Al/C-based FLP **III**, insertion of the isocyanate into the C–Al as well as in the Al–N bond is observed.[31] In the reaction of the geminal Ga/P-based FLP **VI** with phenyl isocyanate, both regioisomers, resulting from insertion of the C=O or the C=N double bond into the ring, can be observed (Scheme 5).[45]

After adding one equivalent of phenyl isocyanate to a solution of **3** in deuterated benzene at room temperature, two new signals at $\delta_{^{31}P}$ = 19.0 and 20.2 ppm appeared in the ^{31}P NMR

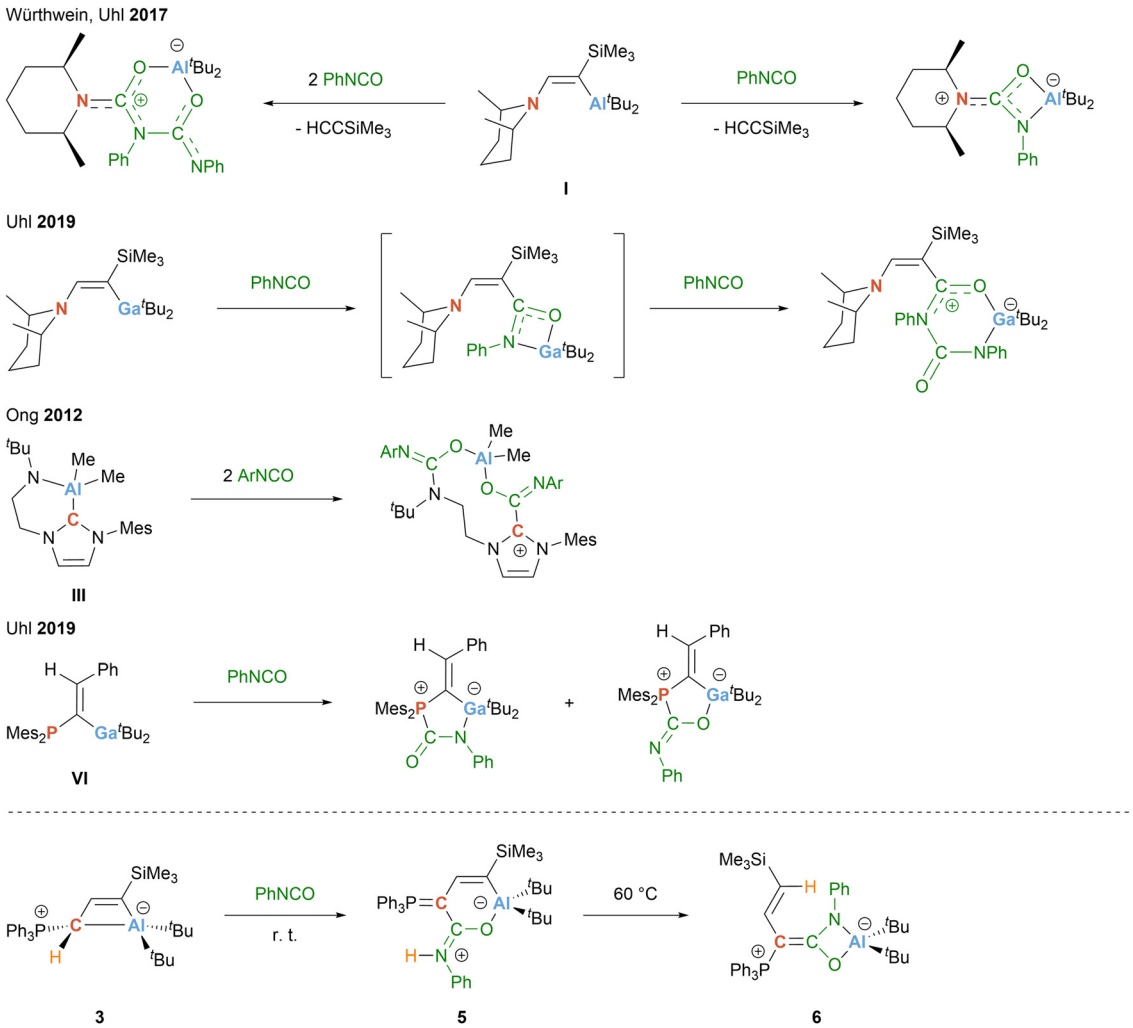

Scheme 5 Top: selected reaction products of E^{13}/E^{15}-based FLPs with isocyanates (Ar = *p*-Tol); bottom: reactivity of **3** towards PhNCO: insertion of C=O into the C–Al bond and proton transfer to N to form **5**. Complete rearrangement of **5** to **6** at 60 °C.

spectrum. When the NMR sample was heated to 60 °C overnight, only the signal at $\delta_{^{31}P}$ = 19.0 ppm remained. The ^{1}H NMR spectra showed a singlet at $\delta_{^{1}H}$ = 5.77 ppm and two doublets of doublets in this region. The singlet vanished upon thermal treatment of the sample, whereas the intensity of the two multiplets increased (see the SI). Since no coupling of the signal at $\delta_{^{1}H}$ = 5.77 ppm to the phosphorus atom could be observed, a proton shift from C1 to another part of the molecule was concluded. From the coupling constant of the two doublets of doublets in the ^{1}H NMR spectrum, the ring extension in an analogous way to the observation with benzaldehyde could be precluded. The high H–H coupling constant of 18.9 Hz indicated an antiperiplanar spatial arrangement of two geminal protons.[46]

Single crystals, obtained after heating the sample to 60 °C, were obtained from a concentrated benzene solution at room temperature. The compound was isolated and assigned to the signal at $\delta_{^{31}P}$ = 19.0 ppm. The molecular structure is depicted in Fig. 7 (space group $P\bar{1}$).

The P1–C1 bond length in **6** is shorter compared to **3** and **4**, indicating a higher double bond character. The C–C bond lengths increase from C2–C3 over C1–C4 to C1–C2, whereas the C2═C3 bond length of 1.339(3) Å is in the range of a typical C═C double bond and the others are between a single and a double bond.[42]

To trap the species that forms first, we dissolved **3** in toluene and cooled the solution down to −30 °C. One equivalent of PhNCO was added and the reaction mixture was stirred for 5 minutes. The reaction mixture was put in a freezer (−30 °C) and after two weeks, colorless crystals formed. The molecular structure obtained from SC-XRD is shown in Fig. 8.

A planar structure can be observed, which features a short C1–C4 bond. The C–C bond lengths increase from C2–C3 (1.3523(18) Å) to C1–C4 (1.4006(17) Å) and then to C1–C2 (1.4781(17) Å). Compared to **4**, the C1–C4 bond is significantly shorter (1.4006(17) Å for **5**, compared to 1.560(3) Å in **4**). Also, the C4–O1 bond is short in **5** (1.2779(15) Å), compared to **4** (1.400(4) Å). The P1–C1 bond length (1.7392(12) Å) is in the same range compared to **3** (1.7341(15) Å), whereas a longer P1–C1 bond is observed for **4** (1.8447(17) Å). The C4–N1 bond length of 1.3644(16) Å is between a single and double bond.[42]

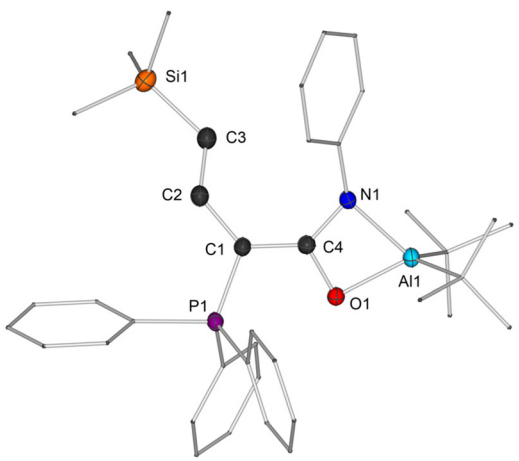

Fig. 7 Molecular structure of **6**. Selected bond lengths (Å) and angles (°): P1–C1: 1.7500(17), C1–C2: 1.463(2), C2–C3: 1.339(3), C1–C4: 1.409(2), N1–C4: 1.348(2), O1–C4: 1.3373(19), Al1–N1: 1.9267(14), Al1–O1: 1.8598(11); C2–C1–C4: 128.02(15), P1–C1–C4: 111.90(12), N1–C4–O1: 108.66(13), N1–Al1–O1: 70.32(5).

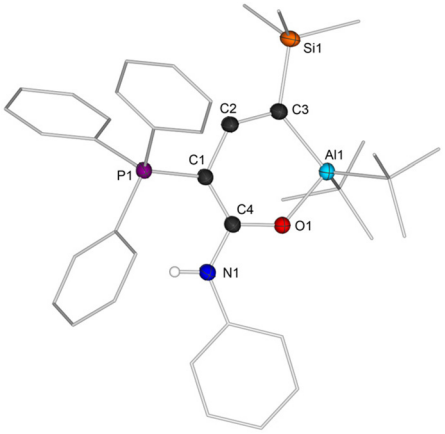

Fig. 8 Molecular structure of **5**. Hydrogen atoms besides H1, the disorder of one *tert*-butyl group and co-crystallized toluene molecules are omitted for clarity. Selected bond lengths (Å) and angles (°): P1–C1: 1.7392(12), C1–C2: 1.4781(17), C2–C3: 1.3523(18), C1–C4: 1.4006(17), N1–C4: 1.3644(16), O1–C4: 1.2779(15), Al1–O1: 1.8386(9), Al1–C3: 1.9718(14); C2–C1–C4: 122.21(11), P1–C1–C4: 126.26(9), N1–C4–O1: 115.81(11), C1–C4–O1: 122.02(11), C3–Al1–O1: 98.02(5).

The trigonal-planar coordination of C1 indicates the shuttling of the ylidic proton to N1. The presence of an N–H bond was confirmed by ^{1}H NMR and IR spectroscopy. In the ^{1}H NMR spectrum of the reaction mixture, the singlet at $\delta_{^{1}H}$ = 5.77 ppm can be assigned to the hydrogen atom now bonded to N1. In the IR spectrum, the N–H absorption band is observed at $\tilde{\nu}$ = 3420 cm^{-1}.

Additional DFT calculations at the PCM-BP86-D3/def2-TZVPP//BP86-D3/def2-SVP level were carried out to explore the mechanism involved in the rearrangement reaction (Fig. 9). Based on the reaction of **3** with benzaldehyde, discussed above, the process can be assumed to begin from the six-membered heterocyclic intermediate **INT1**, whose formation is strongly exergonic (ΔG = −17.2 kcal mol^{-1}). This species evolves into the isolated intermediate **5** in an exergonic reaction (ΔG = −7.1 kcal mol^{-1}), *via* **TS1**, a saddle point associated with the H-migration from the carbon (former ylide) atom to the adjacent nitrogen atom, with an activation barrier of 29.9 kcal mol^{-1}. Species **5** can then be transformed into intermediate **INT2** through **TS2**, a transition state associated with an oxygen-to-nitrogen coordination change at the aluminum center, with a barrier of 29.9 kcal mol^{-1}. Despite that, this process is significantly endergonic (ΔG = 15.0 kcal mol^{-1}), which is consistent with the heating required in the experiments. Alternatively, **INT2** might be directly formed from **INT1′**, the possible isomer of **INT1** having an Al–N bond.

This journal is © The Royal Society of Chemistry 2026

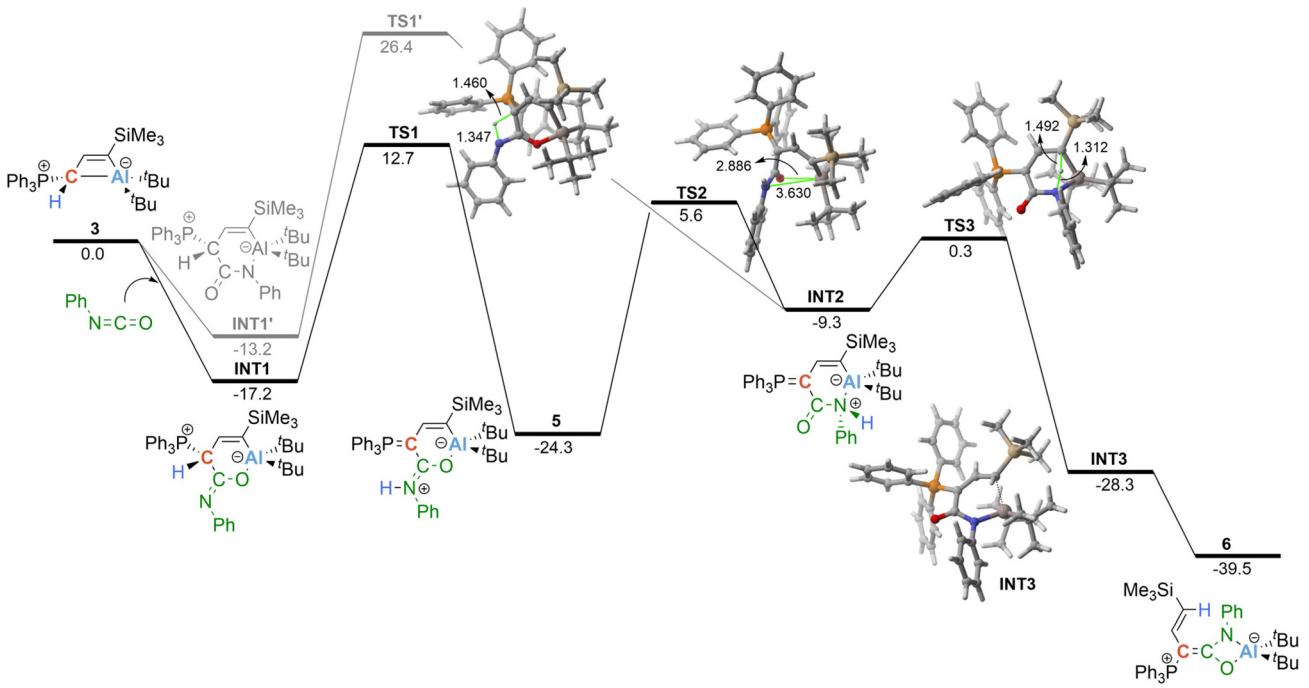

Fig. 9 Computed reaction profile for the reaction of **3** with phenyl isocyanate. Relative free energies (ΔG, 333.15 K) and bond distances are given in kcal mol^{-1} and angstroms, respectively. All data have been computed at the PCM-BP86-D3/def2-TZVPP//BP86-D3/def2-SVP level.

However, the high barrier computed for the corresponding H-migration ($\Delta G^{\neq}$ = 39.6 kcal mol^{-1}, *via* **TS1′**) renders this alternative unfeasible. From **INT2**, a new H-migration from the nitrogen atom to the C(–SiMe$_3$) atom takes place *via* **TS3** ($\Delta G^{\ddagger}$ = 9.3 kcal mol^{-1}) in a highly exergonic reaction (ΔG = −19.0 kcal mol^{-1}) to produce the acyclic intermediate **INT3**. Simple rotation around the (O═)C–N bond allows the coordination of the oxygen atom to the aluminum center, finally affording the observed species **6**.

Conclusions

Herein, we described the synthesis, characterization and reactivity of a phosphorus ylide-derived aluminacyclobutene with Al/C-based ambiphilic reactivity. We showed that the diorganoalanate Li[*t*Bu$_2$AlH$_2$]·2thf, which was structurally characterized, can be used as a combination of a base and hydrometallation reagent to synthesize the title compound *via* hydrometallation. Whereas the reaction of the ambiphile with benzaldehyde afforded a ring expansion product, the reaction with phenyl isocyanate yielded a rearrangement product after heating. This rearrangement includes the initial migration of a proton from the ylidic carbon atom to the isocyanate's nitrogen atom, followed by O-to-N coordination change at the aluminum center and final proton migration to produce an AlOCN heterocycle. The intermediate product was characterized *via* single-crystal XRD. Quantum chemical calculations indicate that the ring expansion product, similar to the reaction product with benzaldehyde, only appears as an initial intermediate, whereas the proton shuttling to the nitrogen atom appears as an intermediate product and the proton shift to C3 yields the rearrangement product as the thermodynamically favoured product.

Experimental

General considerations

All operations were carried out under dry argon using standard Schlenk and glovebox techniques.[47] Li[*t*Bu$_2$AlH$_2$]·2thf was synthesized according to a reported procedure[48] or synthesized *via* the modified procedure described below. Chemicals were purchased from Sigma-Aldrich or abcr. Triphenylphosphine and 3-bromo-1-(trimethylsilyl)-1-propyne were used as purchased. Solvents were dried over Na/K and rigorously degassed before use. Benzaldehyde and phenyl isocyanate were dried over molecular sieves and degassed prior to use. NMR spectra were recorded on a Bruker Avance 300 or Bruker Avance Neo 400 spectrometer operating at ^{1}H Larmor frequencies of 300 or 400 MHz in dry degassed deuterated solvents. ^{1}H, ^{13}C{^{1}H} and ^{29}Si{^{1}H} chemical shifts were reported against TMS, ^{31}P{^{1}H} against H_3PO_4 (85%) and ^{7}Li against LiCl (1 M in D_2O). Coupling constants (J) are given in Hertz as positive values, regardless of their individual signs. IR spectra were recorded on a Bruker Alpha spectrometer using the attenuated total reflection technique (ATR) and the data are quoted in wavenumbers (cm^{-1}). Elemental analyses were carried out in the institutional technical laboratories of the Karlsruhe Institute of Technology (KIT). Elemental analysis data were gathered

from the isolated crystalline material of the corresponding compound and reported as obtained even if the established deviation of ±0.4% was not reached, as these requirements were shown to be misleading in some cases.[49]

Synthesis and characterization of the compounds

Modified procedure for the synthesis of Li[*t*-Bu$_2$AlH$_2$]·2thf (1). A solution of *tert*-butyl lithium (1.7 M in pentane, 20 ml, 34.0 mmol, 1.99 equiv.) was added to a suspension of $LiAlH_4$ (0.65 g, 17.1 mmol, 1.00 equiv.) in THF (25 ml) in an ice bath under rigorous stirring. The reaction mixture was stirred for 16 hours at room temperature and then evaporated to dryness. The residue was extracted with toluene (40 ml) and filtered. The filtrate was dried *in vacuo*. The residue was recrystallized from heptane at −30 °C and dried. The product was obtained as a colorless solid. The analytical data matched those from the literature.[38] **Yield**: 1.69 g, 5.75 mmol, 34%. **^{1}H NMR** (300 MHz, C_6D_6): $\delta_{^1H}$ (ppm) = 3.62–3.46 (m, 8H, OCH_2), 2.82 (s, br, 2H, Li–H–Al), 1.49 (s, 18H, C(CH_3)$_3$), 1.36–1.26 (m, 8H, OCH$_2$CH_2). **^{13}C NMR** (75 MHz, C_6D_6): $\delta_{^{13}C}$ (ppm) = 68.8 (s, O*C*H$_2$), 32.4 (s, C(*C*H$_3$)$_3$), 25.4 (s, OCH$_2$*C*H$_2$), 15.2 (s, br, *C*(CH$_3$)$_3$). **^{7}Li NMR** (117 MHz, C_6D_6): $\delta_{^7Li}$ (ppm) = 0.36 (s).

Synthesis and characterization of [Ph$_3$PCH$_2$C≡CSiMe$_3$][Br] (2). A solution of triphenylphosphine (17.5 g, 66.6 mmol, 1.25 equiv.) in 50 ml of toluene was added to a solution of 3-bromo-1-(trimethylsilyl)-1-propyne (10.18 g, 53.3 mmol, 1.00 equiv.) in 30 ml of toluene. The reaction mixture was stirred for 16 hours. The resulting solid was isolated through filtration and washed with 10 ml of toluene twice and 10 ml of hexane. After drying *in vacuo*, the product was obtained as an off-white powder. **Yield**: 20.0 g, 44.2 mmol, 83%. **^{1}H NMR** (400 MHz, $CDCl_3$): $\delta_{^1H}$ (ppm) = −0.07 (s, 9H, Si–CH_3), 5.13 (d, $^2J_{P-H}$ = 15.1 Hz, 2H, P–CH_2), 7.63–7.69 (m, 6H, *o*-C*H*), 7.76–7.81 (m, 3H, *m*-C*H*), 7.83–7.90 (m, 6H, *p*-C*H*). **^{13}C{^{1}H} NMR** (101 MHz, $CDCl_3$): $\delta_{^{13}C}$ (ppm) = −0.7 (d, $^5J_{P-C}$ = 1.5 Hz, Si–*C*H$_3$), 19.6 (d, $^1J_{P-C}$ = 54.8 Hz, P–*C*H$_2$), 93.0 (d, $^2J_{P-C}$ = 13.1 Hz, CH$_2$–*C*), 94.8 (d, $^3J_{P-C}$ = 8.4 Hz, Si–*C*), 117.6 (d, $^1J_{P-C}$ = 87.5 Hz, i-*C*), 130.3 (d, $^2J_{P-C}$ = 12.9 Hz, *o*-*C*H), 134.1 (d, $^3J_{P-C}$ = 10.0 Hz, *m*-*C*H), 135.3 (d, $^4J_{P-C}$ = 3.2 Hz, *p*-*C*H). **^{29}Si{^{1}H} NMR** (79 MHz, $CDCl_3$): $\delta_{^{29}Si}$ (ppm) = −17.0 (s). **^{31}P{^{1}H} NMR** (162 MHz, $CDCl_3$): $\delta_{^{31}P}$ (ppm) = 22.2 (s). **IR** (ATR): $\tilde{\nu}$ (cm^{-1}) = 3050 (vw), 3006 (vw), 2958 (vw), 2896 (vw), 2804 (w), 2726 (vw), 2476 (vw), 2178 (vw), 1587 (vw), 1482 (vw), 1440 (m), 1393 (vw), 1250 (w), 1185 (vw), 1163 (vw), 1115 (m), 1041 (w), 994 (vw), 840 (vs), 770 (w), 745 (vs), 726 (s), 716 (s), 689 (vs), 639 (m), 617 (vw), 563 (vs), 502 (vs), 492 (vs), 428 (m), 402 (vw), 393 (vw), 381 (vw). **Elemental analysis** (%): found: C, 64.4; H, 5.58. Calc. for $C_{24}H_{26}BrPSi$·0.1 toluene: C, 64.7; H, 5.89%.

Synthesis and characterization of Ph$_3$PCH(CH═CSiMe$_3$)Al*t*Bu$_2$ (3). In a glovebox, **2** (1.00 g, 2.21 mmol, 1.00 equiv.) and Li[^{t}Bu$_2$AlH$_2$]·2thf (649 mg, 2.21 mmol, 1.00 equiv.) were mixed and toluene (40 ml) was added. The reaction mixture turned orange and was stirred overnight. A colorless precipitate formed. The solvent was removed *in vacuo*. The remaining solid was extracted with cyclopentane (40 ml) and filtered. The filtrate was concentrated under reduced pressure and stored at −30 °C. Yellow crystals formed overnight, were separated from the mother liquor and dried *in vacuo*. The product was obtained as an orange solid. Storing the mother liquor at −30 °C yielded an additional amount of the product. **Yield**: 640 mg, 1.24 mmol, 56%. **^{1}H NMR** (300 MHz, C_6D_6): $\delta_{^1H}$ (ppm) = 0.36 (s, 9H, Si(CH_3)$_3$), 1.30 (s, 18H, C(CH_3)$_3$), 3.04 (dd, $^2J_{P-H}$ = 18.1 Hz, $^3J_{H-H}$ = 1.3 Hz, 1H, P–C*H*), 6.93–7.03 (m, 9H, *o*- and *p*-C*H*), 7.37–7.46 (m, 6H, *m*-C*H*), 7.78 (dd, $^3J_{P-H}$ = 3.5 Hz, $^3J_{H-H}$ = 1.3 Hz, 1H, P–CH–C*H*). **^{13}C{^{1}H} NMR** (75 MHz, C_6D_6): $\delta_{^{13}C}$ (ppm) = 0.2 (s, Si(*C*H$_3$)$_3$), 16.8 (s, *C*(CH$_3$)$_3$), 20.9 (d, $^1J_{P-C}$ = 36.7 Hz, P–*C*H), 26.2 (s, Si–*C*–Al), 32.2 (s, C(*C*H$_3$)$_3$), 126.2 (d, $^1J_{P-C}$ = 83.4 Hz, i-*C*), 129.2 (d, $^2J_{P-C}$ = 11.5 Hz, *o*-*C*H), 132.8 (d, $^4J_{P-C}$ = 2.9 Hz, *p*-*C*H), 133.7 (d, $^3J_{P-C}$ = 9.0 Hz, *m*-*C*H), 140.8 (d, $^2J_{P-C}$ = 8.7 Hz, P–CH–*C*H). **^{29}Si{^{1}H} NMR** (79 MHz, C_6D_6): $\delta_{^{29}Si}$ (ppm) = −12.9 (s). **^{31}P{^{1}H} NMR** (121 MHz, C_6D_6): $\delta_{^{31}P}$ (ppm) = 23.1 (s). **IR** (ATR): $\tilde{\nu}$ (cm^{-1}) = 3057 (vw), 2944 (vw), 2860 (vw), 2815 (m), 2749 (vw), 2687 (vw), 1590 (vw), 1504 (w), 1484 (vw), 1461 (w), 1436 (m), 1377 (vw), 1353 (vw), 1332 (vw), 1307 (vw), 1237 (w), 1171 (vw), 1103 (m), 1028 (vw), 997 (w), 945 (m), 898 (vw), 829 (s), 807 (s), 770 (w), 741 (s), 714 (s), 687 (vs), 628 (vw), 583 (s), 553 (s), 537 (vs), 512 (vs), 490 (m), 468 (w), 451 (vw), 426 (m), 396 (w), 379 (vw). **Elemental analysis** (%): found: C, 74.43; H, 8.79. Calc. for $C_{32}H_{44}AlPSi$: C, 74.67; H, 8.62%.

Synthesis and characterization of Ph$_3$PCH(CH═CSiMe$_3$)-{(Ph)C(H)O}Al*t*Bu$_2$ (4). **3** (50.0 mg, 97.1 μmol, 1.00 equiv.) was dissolved in toluene (5 ml). Benzaldehyde (9.91 μl, 10.3 mg, 97.1 μmol, 1.00 equiv.) was added. The reaction mixture turned pale-yellow and was stirred for 8 hours. Afterwards, the solution was concentrated, which led to the formation of a colorless solid. The mother liquor was removed using a syringe. The solid was dried *in vacuo*. **4** was obtained as a colorless solid. **Yield**: 15.0 mg, 24.2 μmol, 25%. **^{1}H NMR** (300 MHz, THF-d_8): $\delta_{^1H}$ (ppm) = −0.14 (s, 9H, Si(CH_3)$_3$), 0.84 (s, 9H, C(CH_3)$_3$), 0.92 (s, 9H, C(CH_3)$_3$), 4.43 (ddd, $^2J_{P-H}$ = 15.5 Hz, $^3J_{H-H}$ = 8.2 Hz, $^3J_{H-H}$ = 2.3 Hz, 1H, P–C*H*), 5.51 (d, $^3J_{H-H}$ = 8.2 Hz, 1H, C^2*H*), 6.75–6.89 (m, 3H, *o*-/*p*-C*H*), 6.99–7.06 (m, 2H, *m*-C*H*), 7.16 (dd, $^3J_{P-H}$ = 13.1 Hz, $^3J_{H-H}$ = 2.2 Hz, 1H, C^4*H*), 7.45–7.55 (m, 6H, *m*-CH_{PPh3}), 7.56–7.70 (m, 9H, *o*-/*p*-CH_{PPh3}). **^{13}C{^{1}H} NMR** (75 MHz, THF-d_8): $\delta_{^{13}C}$ (ppm) = 1.0 (s, Si(*C*H$_3$)$_3$), 16.1 (s, br, *C*(CH$_3$)$_3$), 32.8 (s, C(*C*H$_3$)$_3$), 33.0 (s, C(*C*H$_3$)$_3$), 49.2 (d, J_{P-C} = 30.2 Hz, *C*H$_{arom.}$), 78.6 (*C*^{2}H), 121.7 (d, J_{P-C} = 81.7 Hz, *C*$_{arom.}$), 128.0 (s, *C*H$_{arom.}$), 128.7 (d, J_{P-C} = 16.9 Hz, *C*H$_{arom.}$), 130.5 (d, J_{P-C} = 12.0 Hz, *C*H$_{arom.}$), 134.5 (d, J_{P-C} = 3.0 Hz, *C*H$_{arom.}$), 135.0 (d, J_{P-C} = 8.7 Hz, *C*H$_{arom.}$), 143.9 (s, *C*H–O), 148.1 (s, *C*$_{arom.}$). **^{29}Si{^{1}H} NMR** (79 MHz, THF-d_8): $\delta_{^{29}Si}$ (ppm) = −6.8 (s). **^{31}P{^{1}H} NMR** (121 MHz, THF-d_8): $\delta_{^{31}P}$ (ppm) = 22.5 (s). **IR** (ATR): $\tilde{\nu}$ (cm^{-1}) = 2939 (w), 2859 (vw), 2797 (m), 2740 (vw), 2679 (vw), 1589 (vw), 1513 (vw), 1487 (vw), 1462 (w), 1438 (m), 1373 (vw), 1277 (vw), 1240 (w), 1169 (vw), 1100 (m), 1067 (w), 997 (w), 903 (w), 853 (m), 828 (m), 808 (s), 769 (vw), 740 (s), 687 (vs), 615 (m), 569 (w), 549 (vs), 537 (s), 519 (vs), 432 (s), 396 (vw). **Elemental analysis** (%): found: C, 76.34; H, 7.74. Calc. for $C_{39}H_{50}AlOPSi$: C, 75.45; H, 8.12%.

Synthesis and characterization of Ph$_3$PC(CH═CSiMe$_3$)-{(PhNH)CO}Al*t*Bu$_2$ (5). **3** (24.0 mg, 46.6 μmol, 1.00 equiv.) was dissolved in toluene (0.5 mL) and cooled down to −30 °C.

This journal is © The Royal Society of Chemistry 2026

Phenyl isocyanate (5.55 mg, 5.05 μL, 46.6 μmol, 1.00 equiv.) was added to the solution, which was then stirred for 5 minutes. The reaction mixture was put in a freezer (−30 °C) and after two weeks, colorless crystals formed. The mother liquor was decanted, and the crystals were dried *in vacuo* (*Parenthetic aside*: since **5** already rearranges to **6** at room temperature, no further NMR analysis was possible. The NMR signals are assigned from the product mixture, not from the pure compound. The IR spectrum was also obtained from the product mixture.) **Yield**: 10.0 mg, 15.8 μmol, 34%; purity 70% according to NMR (see the SI). **^{1}H NMR** (400 MHz, C_6D_6): $\delta_{^1H}$ (ppm) = 0.29 (s, 9H, Si(CH_3)$_3$), 1.67 (s, 18H, C(CH_3)$_3$), 5.74 (s, 1H, N*H*), 6.76–6.70 (m, 1H), 6.91–6.82 (m, 6H), 7.00–6.93 (m, 4H), 7.14–7.09 (m, 2H), 7.44–7.36 (m, 6H). **^{31}P{^{1}H} NMR** (162 MHz, C_6D_6): $\delta_{^{31}P}$ (ppm) = 20.2 (s). **IR (ATR):** $\tilde{\nu}$ (cm^{-1}) = 3420 (vw), 2936 (w), 2804 (m), 2745 (vw), 2685 (vw), 1598 (m), 1558 (s), 1510 (m), 1496 (m), 1485 (w), 1472 (w), 1460 (w), 1436 (m), 1427 (m), 1393 (w), 1343 (vs), 1236 (s), 1180 (w), 1128 (vw), 1100 (m), 1083 (w), 1028 (vw), 996 (w), 923 (m), 857 (m), 822 (m), 808 (s), 752 (m), 743 (s), 718 (m), 691 (vs), 642 (vw), 617 (w), 574 (vs), 539 (m), 525 (s), 516 (s), 477 (w), 432 (m).

Synthesis and characterization of Ph$_3$PC(CH═CHSiMe$_3$)-{(Ph)NCO}Al*t*Bu$_2$ (6). PhNCO (21.23 μl, 23.14 mg, 194 μmol, 1.00 equiv.) was added to a solution of **3** (100 mg, 194 μmol, 1.00 equiv.) in toluene (10 ml). The reaction mixture turned slightly yellow. The mixture was stirred at 60 °C for 16 hours. The solution was concentrated and stored at −30 °C, which led to the formation of yellow crystals. The crystals were separated from the mother liquor and dried *in vacuo*. **Yield**: 56 mg, 88.3 μmol, 45%. **^{1}H NMR** (300 MHz, C_6D_6): $\delta_{^1H}$ (ppm) = −0.17 (s, 9H, Si(CH_3)$_3$), 1.23 (s, 18H, C(CH_3)$_3$), 4.94 (dd, $^3J_{H-H}$ = 18.9 Hz, $^4J_{P-H}$ = 2.0 Hz, 1H, Si–C*H*), 6.06 (dd, $^3J_{H-H}$ = 18.9 Hz, $^3J_{P-H}$ = 13.8 Hz, 1H, P–C–C*H*), 6.86–6.93 (m, 1H, *p*-C*H*), 6.95–7.08 (m, 9H, *o*-/*p*-CH_{PPh3}), 7.20–7.26 (m, 2H, *m*-C*H*), 7.31–7.39 (m, 2H, *o*-C*H*), 7.59–7.69 (m, 6H, *m*-C$_{PPh3}$). **^{13}C{^{1}H} NMR** (75 MHz, C_6D_6): $\delta_{^{13}C}$ (ppm) = −0.9 (s, Si(*C*H$_3$)$_3$), 15.8 (s, *C*(CH$_3$)$_3$), 30.5 (s, C(*C*H$_3$)$_3$), 56.9 (d, $^1J_{P-C}$ = 111.7 Hz, P–C), 122.1 (s, *C*H$_{arom.}$), 123.1 (d, $^4J_{P-C}$ = 10.0 Hz, Si–*C*H), 123.5 (s, *C*H$_{arom.}$), 125.9 (s, *C*$_{arom.}$), 127.1 (s, *C*$_{arom.}$), 128.6 (d, J_{P-C} = 6.9 Hz, *C*H$_{arom.}$), 128.8 (d, J_{P-C} = 12.2 Hz, *C*H$_{arom.}$), 132.1 (d, J_{P-C} = 2.9 Hz, *C*H$_{arom.}$), 134.4 (d, J_{P-C} = 9.6 Hz, *C*H$_{arom.}$), 137.8 (d, J_{P-C} = 10.4 Hz, P–C–*C*H), 144.5 (s, *C*$_{arom.}$), 174.0 (d, $^2J_{P-C}$ = 9.3 Hz, N–*C*–O). **^{29}Si{^{1}H} NMR** (79 MHz, C_6D_6): $\delta_{^{29}Si}$ (ppm) = −8.6 (s). **^{31}P{^{1}H} NMR** (121 MHz, C_6D_6): $\delta_{^{31}P}$ (ppm) = 19.0 (s). **IR (ATR):** $\tilde{\nu}$ (cm^{-1}) = 2943 (vw), 2863 (vw), 2811 (w), 1643 (vw), 1602 (w), 1580 (w), 1497 (w), 1484 (vw), 1462 (w), 1435 (m), 1372 (vw), 1307 (vw), 1242 (w), 1164 (vw), 1102 (m), 1064 (w), 1027 (w), 999 (w), 830 (s), 813 (m), 746 (s), 714 (w), 690 (vs), 643 (vw), 582 (w), 515 (s), 465 (vw), 426 (vw), 413 (w), 380 (vw). **Elemental analysis** (%): found: C, 73.72; H, 7.70; N, 2.24. Calc. for $C_{39}H_{49}NOAlSiP$: C, 73.90; H, 7.79; N, 2.21%.

Crystallographic details

Diffraction data were measured using a Stoe IPDS II diffractometer and graphite-monochromated MoK_α (0.71073 Å) radiation or a STOE STADIVARI diffractometer and GaK_α (1.34134 Å) radiation. Absorption corrections were carried out using the STOE LANA[50] software package by scaling the diffraction intensities. The structures were solved in OLEX2 1.5[51] by dual-space direct methods with SHELXT,[52] followed by full-matrix least-squares refinement using SHELXL-2014/7.[53] All non-hydrogen atoms were refined anisotropically. The contribution of the hydrogen atoms, in their calculated positions, was included in the refinement using a riding model. The positions of the hydridic H atoms in **1** and **1b** were taken from a difference Fourier map and refined isotropically. CCDC 2560934 (**1**), 2560937 (**3**), 2560938 (**4**), 2560936 (**5**), 2560939 (**6**) and 2560935 (**1b**, see the SI) contain the SI crystallographic data for this paper.

Computational details

All the calculations reported in this paper were performed with the Gaussian 09 suite of programs.[54] Electron correlation was partially taken into account using the BP86[55,56] functional in conjunction with the D3 dispersion correction suggested by Grimme *et al.*[57] using the standard double-ζ quality def2-SVP[58] basis set for all atoms. Reactants, intermediates, and products were characterized by frequency calculations[59] and have positive definite Hessian matrices. Transition structures (TSs) show only one negative eigenvalue in their diagonalized force constant matrices, and their associated eigenvectors were confirmed to correspond to the motion along the reaction coordinate under consideration using the Intrinsic Reaction Coordinate (IRC) method.[60] Single-point energy refinements were carried out at the same DFT level using the much larger triple-ζ quality def2-TZVPP basis sets. Solvent effects were taken into account using the polarizable continuum model (PCM).[61–63] This level is denoted PCM-BP86-D3/def2-TZVPP//BP86-D3/def2-SVP. The computed thermochemical data were corrected following Grimme's quasi-harmonic (QHA) model for entropy[64] with a frequency cutoff value of 100.0 cm^{-1} using the GoodVibes[65] program at the specified temperature and a standard concentration of 1 M. Quantum Theory of Atoms in Molecules (QTAIM) calculations[66] were carried out at the same level using the optimized BP86-D3BJ/def2-SVP geometries.

Author contributions

F. B. designed and supervised the project. P. W. planned the study, carried out the synthetic work and analysed the spectroscopic data. I. F. performed the computational studies. The original draft was written by P. W. and I. F. The manuscript was finalized by F. B.

Conflicts of interest

There are no conflicts to declare.

Data availability

The data supporting this article have been included as part of the article and its supplementary information (SI). Supplementary information: additional figures to the main text; NMR and IR spectra of the compounds; and details of the crystal structures of the compounds. See DOI: https://doi.org/10.1039/d6dt01434h.

CCDC 2560934–2560939 (**1**, **1b**, **3**, **4**, **5** and **6**) contain the supplementary crystallographic data for this paper.[67a–f]

Acknowledgements

The authors acknowledge support provided by the German Research Foundation (DFG) through grant no. BR 2169/5-1 (535548579). This work was financially supported by the Fonds der Chemischen Industrie through a Kekulé scholarships for P.W. We thank Prof. Dr Dieter Fenske, Dr Olaf Fuhr, Prof. Dr Alexander Hinz and Dr Melina Dilanas for help with SC-XRD. I. F. is grateful for financial support from the Spanish MCIN/AEI/10.13039/501100011033 (PID2022-139318NB-I00). The authors also thank Nicole Klaassen for elemental analysis and Helga Berberich for NMR spectroscopic measurements.

References

1 J. A. Jegier and W. L. Gladfelter, *Coord. Chem. Rev.*, 2000, 206–207.
2 M. M. D. Roy, A. A. Omana, A. S. S. Wilson, M. S. Hill, S. Aldridge and E. Rivard, *Chem. Rev.*, 2021, **121**, 12784–12965.
3 R. F. Nystrom and W. G. Brown, *J. Am. Chem. Soc.*, 1947, **69**, 1197–1199.
4 C. Eaborn, I. B. Gorrell, P. B. Hitchcock and J. D. Smith, *Eur. J. Inorg. Chem.*, 2003, **2003**, 3332–3335.
5 F. Krämer, M. Leskov and F. Breher, *Eur. J. Inorg. Chem.*, 2024, **27**, e202300561.
6 A. Stasch, H. W. Roesky, P. Von Ragué Schleyer and J. Magull, *Angew. Chem., Int. Ed.*, 2003, **42**, 5507–5509.
7 M. Khandelwal, D. R. Powell and R. J. Wehmschulte, *Eur. J. Inorg. Chem.*, 2011, **2011**, 521–526.
8 A. Heine and D. Stalke, *Angew. Chem., Int. Ed. Engl.*, 1992, **31**, 854–855.
9 V. A. Pollard, S. A. Orr, R. McLellan, A. R. Kennedy, E. Hevia and R. E. Mulvey, *Chem. Commun.*, 2018, **54**, 1233–1236.
10 H. Nöth and T. Seifert, *Eur. J. Inorg. Chem.*, 1998, **1998**, 1931–1938.
11 G. H. Spikes, J. C. Fettinger and P. P. Power, *J. Am. Chem. Soc.*, 2005, **127**, 12232–12233.
12 G. C. Welch, R. R. San Juan, J. D. Masuda and D. W. Stephan, *Science*, 2006, **314**, 1124–1126.
13 D. W. Stephan, *Science*, 2016, **354**, aaf7229.
14 D. W. Stephan and G. Erker, *Angew. Chem., Int. Ed.*, 2010, **49**, 46–76.
15 D. W. Stephan and G. Erker, *Angew. Chem., Int. Ed.*, 2015, **54**, 6400–6441.
16 D. W. Stephan, *J. Am. Chem. Soc.*, 2015, **137**, 10018–10032.
17 M. Ghara, H. Mondal, R. Pal and P. K. Chattaraj, *J. Phys. Chem. A*, 2023, **127**, 4561–4582.
18 F. Krämer, *Angew. Chem., Int. Ed.*, 2024, **63**, e202405207.
19 D. W. Stephan, *Acc. Chem. Res.*, 2015, **48**, 306–316.
20 S. A. Weicker and D. W. Stephan, *Bull. Chem. Soc. Jpn.*, 2015, **88**, 1003–1016.
21 K. Lye and R. D. Young, *Chem. Sci.*, 2024, **15**, 2712–2724.
22 K. Liu, T. Liu, X. Wu, X. Jiao, P. Du, J. Wan, T. Heine and L. Liu, *Coord. Chem. Rev.*, 2026, **546**, 217039.
23 A. R. Jupp and D. W. Stephan, *Trends Chem.*, 2019, **1**, 35–48.
24 F.-G. Fontaine and D. W. Stephan, *Philos. Trans. R. Soc., A*, 2017, **375**, 20170004.
25 J. Paradies, *Acc. Chem. Res.*, 2023, **56**, 821–834.
26 T. Holtrichter-Rößmann, C. Rösener, J. Hellmann, W. Uhl, E.-U. Würthwein, R. Fröhlich and B. Wibbeling, *Organometallics*, 2012, **31**, 3272–3283.
27 T. Yanagisawa, Y. Mizuhata and N. Tokitoh, *ChemPlusChem*, 2020, **85**, 933–942.
28 W. Uhl, F. Hengesbach, J. Isermann, M. Soleimani, L. Schürmann, A. Hepp and M. Layh, *Z. Anorg. Allg. Chem.*, 2019, **645**, 1205–1214.
29 C. Appelt, H. Westenberg, F. Bertini, A. W. Ehlers, J. C. Slootweg, K. Lammertsma and W. Uhl, *Angew. Chem., Int. Ed.*, 2011, **50**, 3925–3928.
30 M. E. A. Dilanas and F. Breher, *Eur. J. Inorg. Chem.*, 2025, **28**, e202500174.
31 C.-C. Tai, Y.-T. Chang, J.-H. Tsai, T. Jurca, G. P. A. Yap and T.-G. Ong, *Organometallics*, 2012, **31**, 637–643.
32 V. Dardun, L. Escomel, E. Jeanneau and C. Camp, *Dalton Trans.*, 2018, **47**, 10429–10433.
33 F. Krämer, J. Paradies, I. Fernández and F. Breher, *Nat. Chem.*, 2024, **16**, 63–69.
34 F. Krämer, J. Paradies, I. Fernández and F. Breher, *Chem. – Eur. J.*, 2024, **30**, e202303380.
35 F. Krämer, P. Weisenburger, I. Fernández and F. Breher, *Eur. J. Inorg. Chem.*, 2025, **28**, e202500165.
36 D. González-Pinardo, F. Krämer, F. Breher and I. Fernández, *ChemistryEurope*, 2024, **2**, e202400020.
37 *Modern Ylide Chemistry*, ed. V. H. Gessner, Springer International Publishing, Cham, 2018, vol. 177.
38 C. Eaborn, I. B. Gorrell, P. B. Hitchcock, J. D. Smith and K. Tavakkoli, *Organometallics*, 1994, **13**, 4143–4144.
39 C. Eaborn, I. B. Gorrell, P. B. Hitchcock, J. D. Smith and K. Tavakkoli, *Organometallics*, 1994, **13**, 4143–4144.
40 J. Boudreau, M. A. Courtemanche and F. G. Fontaine, *Chem. Commun.*, 2011, **47**, 11131–11133.
41 J. Boudreau, M. A. Courtemanche, V. M. Marx, D. J. Burnell and F. G. Fontaine, *Chem. Commun.*, 2012, **48**, 11250–11252.
42 P. Pyykko and M. Atsumi, *Chem. – Eur. J.*, 2009, **15**, 12770–12779.

 This journal is © The Royal Society of Chemistry 2026

43 K. Martinewski, T. Holtrichter-Rößmann, C. Rösener, A. Hepp, E. U. Würthwein and W. Uhl, *Chem. – Eur. J.*, 2017, **23**, 6129–6141.

44 M. Radius and F. Breher, *Chem. – Eur. J.*, 2018, **24**, 15744–15749.

45 W. Uhl, J. Possart, A. Hepp and M. Layh, *Z. Anorg. Allg. Chem.*, 2017, **643**, 1016–1029.

46 M. Karplus, *J. Am. Chem. Soc.*, 1963, **85**, 2870–2871.

47 D. F. Shriver and M. A. Drezdzon, *The manipulation of air-sensitive compounds*, John Wiley & Sons, 1986.

48 C. Eaborn, I. B. Gorrell, P. B. Hitchcock, J. D. Smith and K. Tavakkoli, *Organometallics*, 1994, **13**, 4143–4144.

49 R. E. H. Kuveke, L. Barwise, Y. van Ingen, K. Vashisth, N. Roberts, S. S. Chitnis, J. L. Dutton, C. D. Martin and R. L. Melen, *ACS Cent. Sci.*, 2022, **8**, 855–863.

50 J. Koziskova, F. Hahn, J. Richter and J. Kožíšek, *Acta Chim. Slovaca*, 2016, **9**, 136–140.

51 O. V. Dolomanov, L. J. Bourhis, R. J. Gildea, J. A. K. Howard and H. Puschmann, *J. Appl. Crystallogr.*, 2009, **42**, 339–341.

52 G. M. Sheldrick, *Acta Crystallogr., Sect. A: Found. Adv.*, 2015, **71**, 3–8.

53 G. M. Sheldrick, *Acta Crystallogr., Sect. C:Struct. Chem.*, 2015, **71**, 3–8.

54 M. J. Frisch, G. W. Trucks, H. B. Schlegel, G. E. Scuseria, M. A. Robb, J. R. Cheeseman, G. Scalmani, V. Barone, B. Mennucci, G. A. Petersson, H. Nakatsuji, M. Caricato, X. Li, H. P. Hratchian, A. F. Izmaylov, J. Bloino, G. Zheng, J. L. Sonnenberg, M. Hada, M. Ehara, K. Toyota, R. Fukuda, J. Hasegawa, M. Ishida, T. Nakajima, Y. Honda, O. Kitao, H. Nakai, T. Vreven, J. A. Montgomery Jr., J. E. Peralta, F. Ogliaro, M. Bearpark, J. J. Heyd, E. Brothers, K. N. Kudin, V. N. Staroverov, R. Kobayashi, J. Normand, K. Raghavachari, A. Rendell, J. C. Burant, S. S. Iyengar, J. Tomasi, M. Cossi, N. Rega, J. M. Millam, M. Klene, J. E. Knox, J. B. Cross, V. Bakken, C. Adamo, J. Jaramillo, R. Gomperts, R. E. Stratmann, O. Yazyev, A. J. Austin, R. Cammi, C. Pomelli, J. W. Ochterski, R. L. Martin, K. Morokuma, V. G. Zakrewski, G. A. Voth, P. Salvador, J. J. Dannenberg, S. Dapprich, A. D. Daniels, Ö. Farkas, J. B. Foresman, J. V. Ortiz, J. Cioslowski and D. J. Fox, *Gaussian 09, Revision D.01*, Gaussian, Inc., Wallingford CT, 2009.

55 A. D. Becke, *J. Chem. Phys.*, 1993, **98**, 5648–5652.

56 J. P. Perdew, *Phys. Rev. B:Condens. Matter Mater. Phys.*, 1986, **33**, 8822–8824.

57 S. Grimme, J. Antony, S. Ehrlich and H. Krieg, *J. Chem. Phys.*, 2010, **132**, 154104.

58 F. Weigend and R. Ahlrichs, *Phys. Chem. Chem. Phys.*, 2005, **7**, 3297–3305.

59 J. W. McIver and A. Komornicki, *J. Am. Chem. Soc.*, 1972, **94**, 2625–2633.

60 C. Gonzalez and H. B. Schlegel, *J. Phys. Chem.*, 1990, **94**, 5523–5527.

61 S. Miertuš, E. Scrocco and J. Tomasi, *Chem. Phys.*, 1981, **55**, 117–129.

62 J. L. Pascual-ahuir, E. Silla and I. Tuñon, *J. Comput. Chem.*, 1994, **15**, 1127–1138.

63 V. Barone and M. Cossi, *J. Phys. Chem. A*, 1998, **102**, 1995–2001.

64 S. Grimme, *Chem. – Eur. J.*, 2012, **18**, 9955–9964.

65 G. Luchini, J. V. Alegre-Requena, I. Funes-Ardoiz and R. S. Paton, *F1000Research*, 2020, **9**, 291.

66 R. F. W. Bader, *Atoms in Molecules: A Quantum Theory*, Clarendon Press, Oxford, U. K., 1990.

67 (*a*) CCDC 2560934: Experimental Crystal Structure Determination, 2026, DOI: 10.5517/ccdc.csd.cc2ryvsc; (*b*) CCDC 2560935: Experimental Crystal Structure Determination, 2026, DOI: 10.5517/ccdc.csd.cc2ryvtd; (*c*) CCDC 2560936: Experimental Crystal Structure Determination, 2026, DOI: 10.5517/ccdc.csd.cc2ryvvf; (*d*) CCDC 2560937: Experimental Crystal Structure Determination, 2026, DOI: 10.5517/ccdc.csd.cc2ryvwg; (*e*) CCDC 2560938: Experimental Crystal Structure Determination, 2026, DOI: 10.5517/ccdc.csd.cc2ryvxh; (*f*) CCDC 2560939: Experimental Crystal Structure Determination, 2026, DOI: 10.5517/ccdc.csd.cc2ryvyj.